Title
The water dimer I: Experimental characterization

Authors
Mukhopadhyay, Anamika
Cole, William TS
Saykally, Richard J

Publication Date
2015-07-01

DOI
10.1016/j.cplett.2015.04.016

Peer reviewed

Chemical Physics Letters 633 (2015) 13–26

Contents lists available at ScienceDirect

Chemical Physics Letters

journal homepage: www.elsevier.com/locate/cplett

The water dimer I: Experimental characterization

Anamika Mukhopadhyay, William T.S. Cole, Richard J. Saykally*

Department of Chemistry, University of California, Berkeley, CA 94720-1460, United States

ARTICLE INFO

Article history:
Received 11 November 2014
In final form 8 April 2015
Available online 9 May 2015

ABSTRACT

As the archetype of water hydrogen bonding, the water dimer has been studied extensively by both theory and experiment for nearly seven decades. In this article, we present a detailed chronological review of the experimental dimer studies and the insights into the complex nature of water and hydrogen bonding gained from them. A subsequent letter will review the corresponding theoretical advances.

1. Introduction

The quest for an accurate description of water in its myriad forms has preoccupied scientists for centuries. Because it has long been realized that most of the cohesive energy of bulk phases of water comprises a sum over two-body interactions, a thorough and precise description of the hydrogen bonding between just two water molecules is clearly a necessary starting point. Hence, the water dimer has been the focus of a great many theoretical and experimental studies. But the deceptive complexity of this archetype of the hydrogen bond continues to make the long-sought definitive characterization elusive. Here we present a brief review of the published experimental work on the dimer and some related systems. We follow an essentially chronological order, with emphasis on results from Berkeley studies. However, in order to establish the language employed, we first describe the structure and hydrogen bond tunneling dynamics that dominate the dimer spectra that have been observed.

The experimentally determined 'trans-linear' structure is shown in Figure 1, the three feasible tunneling pathways and the associated rotation-tunneling (RT) energy level diagram for the vibrational ground state are depicted in Figure 2. The structure requires six global(Jacobi) coordinates(five angles and one distance) to completely specify the relative orientation of two rigid water molecules, if the water molecules are allowed to be nonrigid, six more(internal) coordinates are required. Hence, the tunneling dynamics described ultimately occur on a 12-dimensional potential energy surface.

2. Matrix isolation spectroscopy

The first spectroscopic observation of the water dimer was made at Berkeley by George Pimentel and co-workers in 1957 [1]. Mid-infrared absorption spectra of trapped water monomers, dimers and higher order clusters were recorded in a solid N_2 matrix at 20 K. Infrared spectral shifts observed for various N_2/H_2O ratios ($N_2/H_2O = 10–1000$) revealed the structure and size of clusters in the matrix. Two salient features observed in O—H stretching region were assigned to the water dimer, one at 3691 and the other at 3546 cm^{-1}. A cyclic structure of the water dimer yielded the best agreement with these experiments, as compared to open-chain or bifurcated structures (Figure 3).

Subsequently, several other groups studied the mid- and near-infrared spectra of water dimers in various cryogenic matrices [2–8]. Tursi et al. [2] and Fredin et al. [3], using a higher resolution spectrometer (1.5–1.0 cm^{-1} spectral slit width in the region of 3700–1150 cm^{-1}), found four peaks in the O—H stretching region of water and assigned them to a singly hydrogen bonded open dimer structure. Two stretching frequencies occurring close to monomer peaks were assigned as the symmetric and antisymmetric stretching bands of the proton-acceptor, and the other two were assigned to hydrogen bonded and free O—H stretching modes of the proton donor counterpart.

In rare gas matrices, water molecules rotate freely, whereas such rotation is hindered in a nitrogen matrix [5–10]. These rare gas studies indicated a bifurcated hydrogen bonded structure for the water dimer under the experimental conditions. Figure 4 shows these possible structures determined by early matrix studies.

Overtone spectra of water and its polymers in the near-infrared region have also been recorded in various matrices [11,12]. In a nitrogen matrix, Perchard found three IR features assignable to water dimer overtone modes [9,10]. Two of them were assigned to symmetric and antisymmetric stretching vibrations in combination

* Corresponding author.
E-mail address: saykally@berkeley.edu (R.J. Saykally).

http://dx.doi.org/10.1016/j.cplett.2015.04.016
0009-2614/

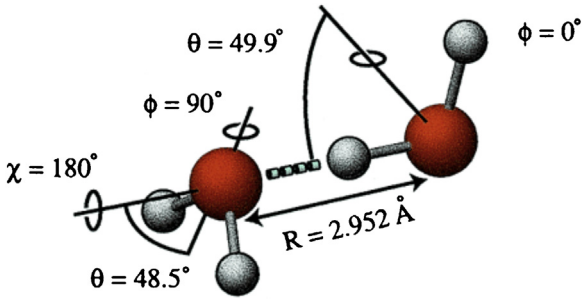

Figure 1. Water dimer-archetype of the aqueous hydrogen bond. The '*trans*-linear' equilibrium structure of the water dimer from the fitted VRT(ASP-W)-II potential surface. The hydrogen bond deviates ~2° from linearity, the O···O distance is 2.95 Å, and the bond strength, D_0, is 3.40 kcal/mol. The monomer on the right acts as a single hydrogen bond donor (D), while that on the left is a single acceptor (A). The highly nonrigid dimer has six floppy intermolecular vibrations, corresponding to the five angles and single distance required to specify the relative orientation of two rigid water molecules.
From Ref. [36].

with the nitrogen stretching mode for the proton acceptor, while the third was assigned as the antisymmetric proton donor stretching band in combination with the matrix nitrogen stretch.

In 2008, normal mode intensities of all intra- and most of the inter-molecular modes of the dimer were measured by Ceponkus et al. and the results were compared with DFT calculations [13]. Ceponkus et al. using their Bruker HR120 FTIR spectrometer (0.1 cm^{-1} resolution for mid-infrared and 1.0 cm^{-1} resolution below 650 cm^{-1}), recorded spectra of the water dimer and its isotopologues in the frequency range of 20–5000 cm^{-1} in both Ne (10 K) and p-H_2 (2.8 K) matrices [14,15]. Seven intermolecular vibrations of the dimer were detected below 600 cm^{-1} with the use of a liquid He cooled Si bolometer. The highest frequency intermolecular vibration appeared at 522.4 cm^{-1}, which was assigned to an out of plane shear vibration of the proton donor of $(H_2O)_2$. The hydrogen bond stretching fundamental was observed at 173 cm^{-1} in a Ne matrix, but was absent in p-H_2 matrix. The p-H_2 matrix data, in combination with DFT/B3LYP/6-311++G(3df,3pd) level of theory, were used to establish the far-infrared band strength for the water dimer [12]. Later, Ceponkus et al. showed that a fine structure appearing in the mid-infrared region in different matrices (Ne, Ar, Kr, p-H_2) cooled to 10 K could be attributed to the acceptor switching motion of the dimer [16]. The observed acceptor switching splitting in different matrices were between one half and one third of the value currently obtained in gas phase studies.

In a recent study of water dimers in a solid hydrogen matrix, Ceponkus et al. found that water rotates freely in solid o-D_2 and p-H_2 matrices but exhibits only librational motion in n-H_2 and n-D_2 matrices [17]. In 2011, Sliter et al. found that nuclear spin conversion is faster for dimeric water than for water monomers confined in a solid Ar matrix at 4 K [18]. In the same year, Tremblay et al. rationalized some weak transitions observed in the near-infrared region for water in inert gas matrices as being due to simultaneous transitions of both proton donor and acceptor normal modes [19]. Intensities of simultaneous transitions increase due to vibrational resonance with the combination mode of the proton donor.

In 2013, Ceponkus et al. reviewed previous matrix isolation studies of water dimers, including their own work performed at Lund [20,21]. Low frequency intermolecular vibrations of the water dimer in inert gas matrices (Ne, Ar, Kr and p-H_2) showed a typical 10–20 cm^{-1} blue shift compared to corresponding gas phase frequencies. This behavior was attributed to the repulsive interaction between water molecules and the matrix. Intensities of hydrogen vibrational bands were used to determine p-H_2 matrix thickness, which yielded water cluster concentrations and intensities of cluster vibrations. Intensity enhancement of the hydrogen bonded O—H stretching vibration was in good agreement with the calculated value obtained by the DFT level of theory. On the other hand, the band intensity of the intermolecular hydrogen bond stretching of $(H_2O)_2$ was overestimated by the same level of calculation.

Matrix studies continue to be of great interest due to their ability to approximately locate prominent intermolecular vibrations and to determine vibrational band intensities. Historically, the structure of the dimer has also been elucidated via matrix experiments, however high resolution VRT and microwave studies have now superseded matrix studies in this regard.

3. Microwave and sub-millimeter spectroscopy of the water dimer

The first high resolution spectra of the water dimer were observed in 1974 by Dyke et al. [22] who measured over 50 RT transitions in the spectral range of 8–50 GHz for both $(H_2O)_2$ and $(D_2O)_2$ dimers, employing a molecular beam electric resonance spectrometer. The (B + C)/2 value for $(H_2O)_2$ obtained from analysis of two $K = 2$ $J = 2 \rightarrow 3$ and $J = 3 \rightarrow 4$ transitions were 6155 MHz and 6144 MHz, respectively. The rich spectrum indicated large amplitude tunneling motions. A near-linear dimer geometry (relative angle of 10° between two monomers) with an equilibrium R_{OO} distance of 2.98 ± 0.04 Å was extracted from these experiments. In a subsequent 1977 letter, Dyke presented a group theoretical representation of the water dimer RT energy levels to characterize the different types of tunneling splittings that were possible in the microwave spectrum [23]. He classified the symmetries of all RT levels and concluded that the a-type spectrum ($\Delta K = 0$) contains both pure rotational and rotational-tunneling transitions. In the same year, Dyke et al. reported additional radio-frequency and microwave transitions for several isotopes i.e. $(H_2{}^{16}O)_2$, $(D_2{}^{16}O)_2$, $(H_2{}^{18}O)_2$, using their molecular beam electric resonance spectrometer [24]. The average dimer structure extracted by fitting pure rotational transitions in the vibrational ground state with a rigid rotor model was also near-linear with an equilibrium R_{OO} distance of 2.98 Å. The proton acceptor molecule is essentially tetrahedrally oriented, making an angle of 58° with respect to O—O axis. The hydrogen bond distance in gas phase dimer was somewhat larger than that found in solid phases, attributed to the cooperative(i.e. many-body) nature of hydrogen bonding. In 1980, Odutola and Dyke reported microwave spectra for several partially deuterated dimers in the region of 10.5–12.5 GHz, for $J = 1 \rightarrow 0$ transitions [25]. They used argon as cooling gas and obtained a rotational temperature of 20 K, colder than in previous studies. The improved signal-to-noise ratio at this low temperature facilitated resolution of proton hyperfine splittings. The R_{OO} distance obtained by fitting the rotational transitions with a rigid rotor model was 2.976 Å. In 1987, Coudert et al. presented Fourier transform microwave spectra of $(H_2O)_2$ and several deuterated species in the frequency range of 7–25 GHz [26]. They reported measurements on ten $K = 1$ lines, of which six were Q-type ($\Delta J = 0$) and four were R ($\Delta J = +1$) type, observing a decrease in donor-acceptor interchange tunneling splitting from 19.5 GHz ($K = 0$) to 16.2 GHz in the $K = 1$ level. In the subsequent year, Dyke and co-workers reported additional rotational-tunneling spectra in the $K = 0$ states for both $(H_2O)_2$ and $(D_2O)_2$ in the radio-frequency and microwave region [27]. With a 3 kHz spectral linewidth in the RF region, highly detailed nuclear hyperfine splitting was resolved. In case of $(H_2O)_2$ and $(D_2O)_2$ dimers, 19,526.73 MHz and 1172.23 MHz were the measured donor-acceptor interchange tunneling splittings for $K = 0$ level, respectively. This result is intuitively consistent with the dependence of the tunneling barrier with particle mass. Odutola et al. in 1988 reported the observation and assignment

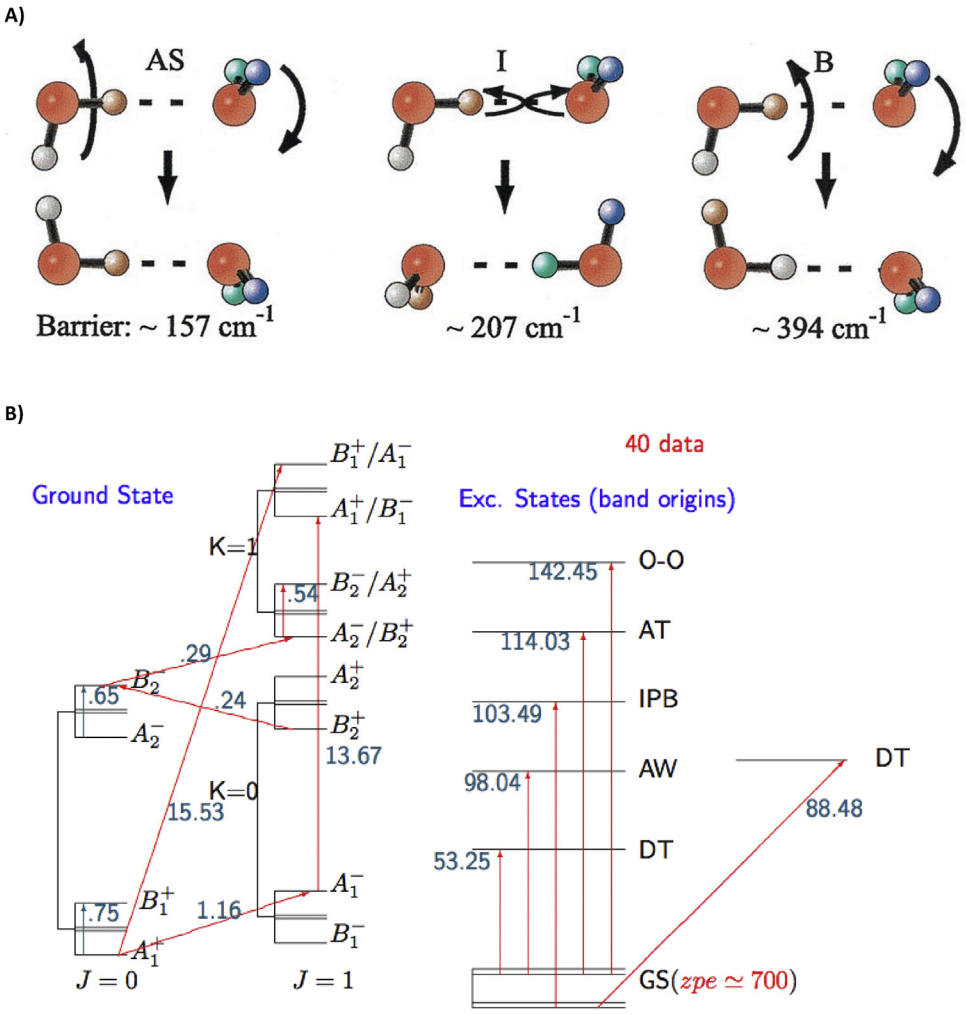

Figure 2. Tunneling pathways and energy levels for the water dimer. (A) The water dimer exhibits three distinct low barrier tunneling pathways that rearrange the hydrogen bonding pattern and induce a sixfold splitting of the vibration-rotation energy levels. Acceptor switching (AS) has the lowest barrier, estimated at 157 cm^{-1} by VRT(ASP-W). This tunneling pathway exchanges the two protons in the hydrogen bond acceptor (A) monomer and begins with a flip of the acceptor followed by a rotation of the donor (D) monomer around its donating O—H bond, and is completed by a 180° rotation of the complex about the O—O bond. The tunneling motion splits each rovibrational energy level into two. Interchange tunneling (I) exchanges the roles of the donor and acceptor water monomers. Several possible pathways exist for this exchange, the lowest barrier path being the geared interchange motion. This pathway begins with a rotation of the donor in the θD angle and rotation of the acceptor about its $C2$ axis to form a trans transition state structure. This is followed by a rotation of the initial donor about its $C2$ axis and a rotation of the initial acceptor in the θA angle such that it becomes the donor. The pathway is completed by a 180° end-over-end rotation of the complex. Calculations with the VRT(ASP-W) potential determine the barrier to be 207 cm^{-1}. The anti-geared interchange pathway also has been determined to be important and is similar to the geared pathway except that it has a cis transition state. The tunneling motion splits each energy level by a much smaller amount than the acceptor switching, resulting into two sets of three energy levels. The bifurcation tunneling motion B, wherein the donor exchanges its protons, comprises the simultaneous in-plane librational motion of the donor with a flip of the acceptor. This is the highest barrier tunneling pathway [394 cm^{-1} with VRT(ASP-W)] resulting only in a small shift of the energy levels, with no additional splitting. (B) Associated energy level diagram showing the tunneling splittings and some rotation-tunneling(RT) transitions for the ground vibrational state, as well as the 5 intermolecular vibrational states that have been measured(DT = donor torsion, AW = acceptor wag, AT = acceptor twist, O—O = oxygen–oxygen, stretch IP = in-plane bend), with all energies given in wavenumbers. The RT splittings vary strongly with vibrational state. The shown splittings are given in cm^{-1}. As an additional note the energy levels between $A^{+/-}$ and $B^{+/-}$ are labeled $E^{+/-}$ in practice but are excluded in the figure due to space constraints. The E levels are doubly degenerate. Red arrows represent allowed transition between energy levels.

of $K = 0$ rotation-tunneling states of $(H_2O)_2$ and $(D_2O)_2$ in the rf and microwave region using the same spectroscopic technique. Population of only the lowest few rotational levels was achieved by expanding 1000 Torr of argon mixed with 2% water through a 25 μm orifice. The donor-acceptor interchange tunneling splittings for $(H_2O)_2$ and $(D_2O)_2$ were extracted as 19,526.73 MHz and 1172.23 MHz, respectively. The effect of rotational-tunneling splitting is more significant on the $(H_2O)_2$ rotational constant than on that of $(D_2O)_2$.

In 1989, Fraser, Suenram, and Coudert measured microwave spectra of $(H_2O)_2$ in the range of 14–110 GHz using an electric-resonance optothermal spectrometer [28]. With the resulting high sensitivity and broad spectral coverage, they were able to observe the $A_1^{\pm}$ states and c-type $K_a = 1$–0 band for $A_2^{\pm}$ and $B_2^{\pm}$ states. They obtained the ground vibrational state ($A_1^{\pm}/B_1^{\pm}$) tunneling splitting for $J = 0$, $K = 0$ as 22.6 GHz and the separation of $K_a = 1$–0 $A_2^{\pm}/B_2^{\pm}$ as 27 GHz. This measured value of interchange tunneling splitting differs from the $J = 1$, $K = 1$ splitting obtained by Coudert et al. and the discrepancy was attributed to the nonrigidity of the dimer.

In 1990 Zwart et al. measured sub-millimeter transitions from $K_a = 1 \rightarrow K_a = 2$ of $(D_2O)_2$ in the region of 350–430 GHz using a slit nozzle expansion [29]. Four bands were observed with Q and R branches. The four bands were fitted with a near-prolate symmetric top model as c-type transitions. The value of the A constant was determined as 120,327.492(32) MHz, and values of other molecular constants were also determined. Subsequently, Zwart et al. measured rotation-tunneling spectra of $(H_2O)_2$ by a direct absorption technique in a continuous slit nozzle (4 cm long and

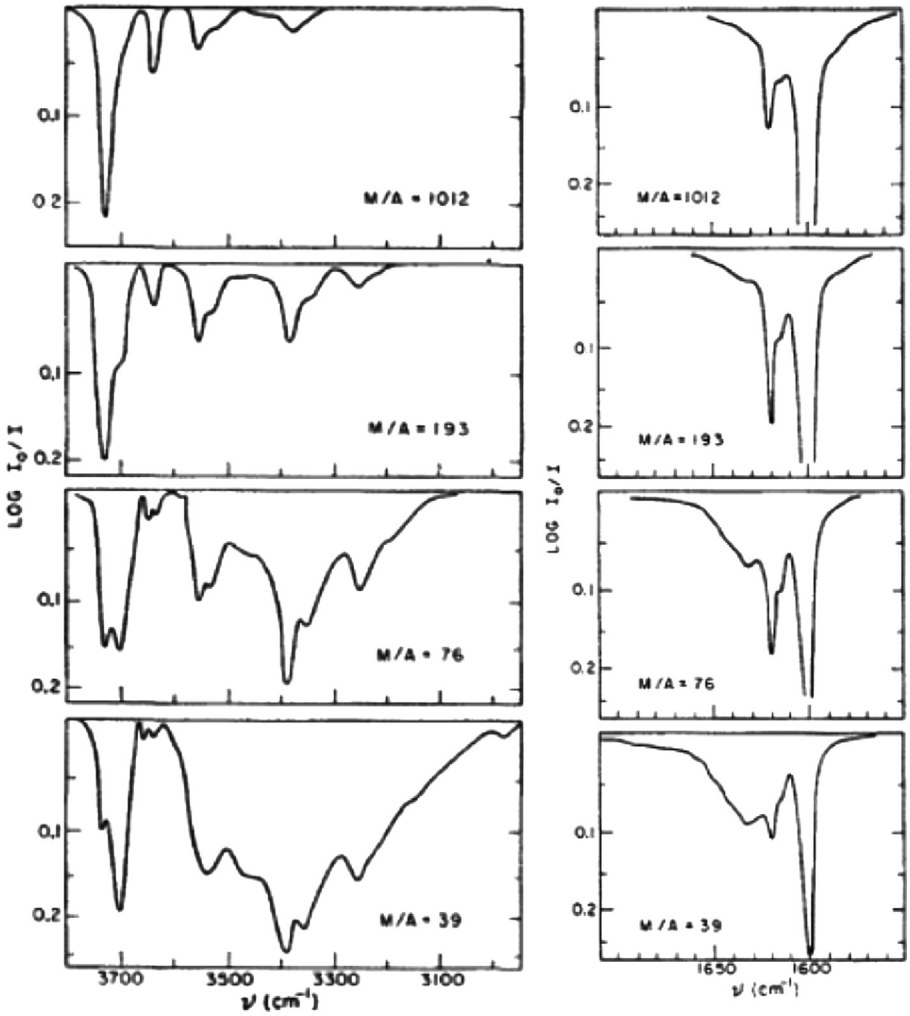

Figure 3. Mid-IR spectra of water trapped in solid nitrogen matrices. Recorded at various nitrogen to water ratios (M = moles Nitrogen, A = moles Water). The LHS represents the spectra at O—H stretching fundamental vibration region and the RHS represents the H—O—H bending region of water.

Plausible structures for dimeric water.

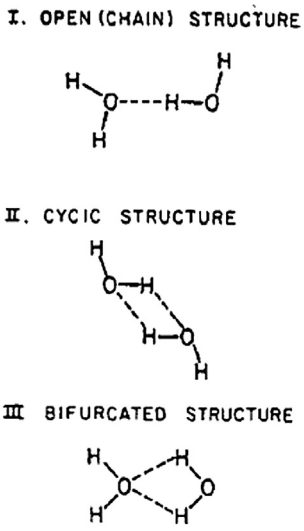

Figure 4. Proposed structures for the water dimer. Deduced from early matrix experiments. Taken with permission from Ref. [1].

25–50 μm wide) expansion, with the aim of precisely determining the value of A and the magnitude of largest tunneling splitting due to 180° rotation of the acceptor monomer ('acceptor switching') [30]. Transitions from $K_a = 0$ (lower) $\rightarrow K_a = 1$(upper) and $K_a = 1$(lower) $\rightarrow K_a = 2$(upper) were observed. The value extracted by fitting the experimental data with an IAM-like treatment for A and the $1 \rightarrow 4$ tunneling splitting (largest) were 227,580.432 MHz and −70,128.436 MHz with an uncertainty of 0.50 and 0.10 MHz, respectively. This improvement in precision was attributed to the incorporation of three additional $\Delta K_a = 1$ subbands in the analysis. In 1997, Fraser et al. reported measurements of microwave and sub-millimeter wave rotational spectra of 12 mixed deuterated-protonated isotopomers of the water dimer up to 460 GHz [31], using a molecular-beam electric resonance optothermal spectrometer which employed a 40 μm pinhole nozzle. Both Ar and He—Ne mixtures were used as the carrier gas with a backing pressure of 300 kPa, and both a-type $\Delta K_a = 0$ ($K_a = 0$–0 and $K_a = 1$–1) and b and c-type $\Delta K_a = 1$ ($K_a = 1$–0) transitions were observed. The value of the tunneling splitting for $J = 0$ was extracted from experiment as 3.59 cm^{-1} for HDO-DOD, but a smaller value (2.6(4) cm^{-1}) was obtained by Gregory and Clary via Monte Carlo calculations.

In 2007, Coudert et al. observed hyperfine splittings for $J \leq 2$ rotation-tunneling sublevels using a FT-MW spectrometer for $(H_2O)_2$ [32]. The hyperfine energy levels were calculated using a Hamiltonian consisting of magnetic spin-rotation and spin–spin terms, simplified using symmetry adapted operators of the G_{16} CNPI group. They found that the hyperfine energies obtained using symmetry adapted rovibrational and nuclear wavefunctions yielded a satisfactory match with the experiment.

The first definitive observation of water dimers in equilibrium water vapor at room temperature was reported by Tretyakov et al. in 2013 [33]. The dimer absorption was recorded in the range of 100–150 GHz at 13 Torr pressure and 296 K using a high-Q Fabry–Perot resonator spectrometer. The water monomer shows a few weak, narrow lines in this region, corresponding to HDO and the excited bending state of $H_2{}^{16}O$. Four equally spaced broad features (due to unresolved transitions) were observed, the center positions of which are separated by $2B_{eff}$ and these were assigned to the water dimer based on the previous supersonic jet measurements. These equidistant rigid rotor-type features actually correspond to E_1 type rotational transitions which are affected relatively weakly by dimer internal rotation and produce a series of $J+1 \leftarrow J, K=0$ transitions]. The ab initio-based dimer spectra exhibit a factor of four smaller effective linewidth than the experimental data. This discrepancy between experiment and calculation was attributed to the use of a simple symmetric top approximation in the latter case (in contrast to a prolate symmetric top approximation). The authors concluded that some low-frequency vibrational modes, which can be populated at room temperature, probably contribute to the water dimer rotational transitions, resulting in the broad features. On the other hand, the intensities of experimental spectra match well with the calculated amplitudes, and the relative abundance of dimer extracted from calculations was about 1.0×10^{-3}. Saykally wrote an invited article on Tretyekov et al.'s observation of water dimer in vapor phase [34]. He emphasized that the surprising regularity in spectral shift and the four times broader spectral linewidth of observed features compared to ab initio calculations needs to be addressed accurately by the authors. He also pointed out that consideration of collisional broadening to characterize water dimer vapor phase spectra would be of much interest.

Early in 2014, Leforestier and co-workers developed a simple model, based on *ab-initio* calculations, to fit experimental millimeter-wave spectra of the water dimer recorded in a wide range of pressure and temperature [35]. Modeling the dimer spectrum in the range of 60–350 GHz, the whole spectrum is divided according to the type of transition. Spectra associated with the transition between levels with A and B symmetries are denoted the 'A + B spectrum', which has several irregular patterns and that of E symmetry (the 'E spectrum') contains regular transitions. The temperature and pressure effect was considered using empirical power laws as $(T_0/T)^{x1}$ and $(P_0/P)^{x2}$, where $x1 = 10.67$ determined by Scribano and Leforestier and $x2 = 2$. Also, $T_0 = 296$ K and $P_0 = 13$ Torr. The dimer spectrum obtained using this model yielded good agreement with the experimental spectra recorded in 110–150 GHz and 190–250 GHz regions.

MW spectroscopy provided the first definitive determination of the dimer ground state energy level structure and provided a measure of the rotation-tunneling motion. This data in combination with the vibrational–rotational transitions outlined in a later section provide the most complete characterization of the dimer potential energy surface. The recent observation of water dimer in the vapor is of great experimental and theoretical interest and should be enlightening as to the role of the dimer in water vapor.

4. Gas phase IR spectroscopy of the water dimer

Keutsch et al. presented an overview of mid-infrared spectroscopy of gas phase free water clusters in a 2003 review article [36]. The study of water cluster IR spectra in supersonic molecular beams was initiated by Vernon et al. and Page et al. in the Y.T. Lee group at Berkeley [37,38]. With the use of supersonic molecular beams the selective control of the cluster species could be achieved, and allowed researchers to focus on particular cluster

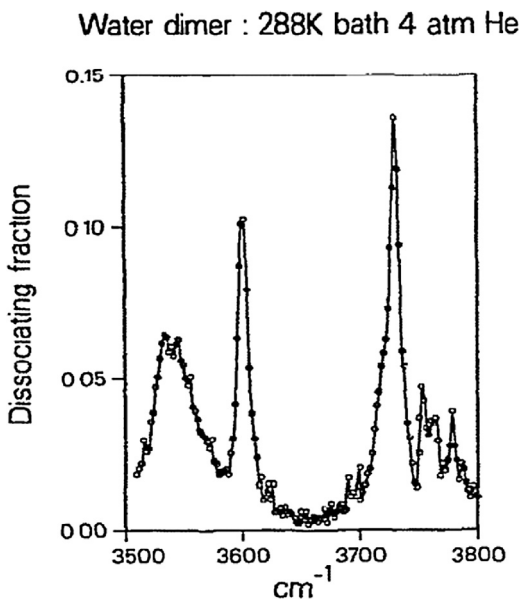

Figure 5. IR vibrational predissociation spectra of the water dimer. Taken in a supersonic molecular beam. The dominant peaks of the spectra were assigned as follows: 3545 $cm^{-1} \rightarrow \upsilon 1$ (donor), 3600 $cm^{-1} \rightarrow \upsilon 1$ (acceptor), 3730 $cm^{-1} \rightarrow \upsilon 3$ (acceptor), 3715 $cm^{-1} \rightarrow \upsilon 3$ (donor). All peaks were shifted greater than 20 cm^{-1} from the matrix results.

Reproduced with permission from Ref. [38].

sizes. Infrared absorption spectra of water polymers $(H_2O)_n$, $n = 1$–5 were recorded by detecting the recoiling off-axis fragments with angle-resolved mass spectrometry, wherein the fragments were produced by vibrational predissociation following the absorption of infrared laser radiation (2900–3750 cm^{-1}). Page et al. [38] focused mainly on the hydrogen bonded water dimers formed in the molecular beam under optimized conditions (Figure 5).

They found four peaks in the fundamental O—H stretching region of water, and assigned them to symmetric and antisymmetric stretching bands of donor and acceptor molecules of the dimer. The broad peak near 3545 cm^{-1}, significantly red-shifted from the monomer peak, was assigned to the hydrogen bonded O—H stretch. In later work, Coker et al. found four water dimer peaks similar to those observed by Page et al. [39]. Their assignment of dimer peaks was supported by quantum chemical calculations reported in the same article. Several different potential surfaces were used to predict the sensitivity of the experimental data, and the best agreement was obtained with RWK2 potential [40].

Huisken et al. used their molecular beam depletion technique in combination with cluster size selection to observe two peaks at 3750 and 3601 cm^{-1}, which were assigned to free and bonded O—H stretching frequencies of water dimer, respectively [41]. Notably, their assignment of the bonded O—H stretching band was in conflict with the work of Page et al. [38], Coker et al. [39] and Huang et al. [42]. Briefly, Huisken et al. presented evidence that the bonded OH stretch previously assigned at 3554 cm^{-1} was in error and reassigned the stretch to 3601 cm^{-1}. Furthermore, band at 3554 cm^{-1} was theorized to originate from a water trimer.

In 1997, Paul et al. measured direct absorption spectra of water clusters (both $(H_2O)_2$ and $(D_2O)_2$) using a pulsed molecular beam source in combination with the newly developed infrared cavity ringdown absorption technique at Berkeley [43,44]. They were able to record rotationally resolved bands for bonded and free O—D stretch vibrational frequencies of the $(D_2O)_2$ dimer. All other higher clusters observed were not rotationally resolved because of vibrational predissociation. In 1999, Paul et al. performed the first measurement of H_2O monomer bending vibrations in gaseous

water clusters, observing discrete blue-shifted bands near 6 μm for clusters up to tetramers [45]. Parallel H_2O bands were measured at 1600.6, 1613.8, 1614.7, and 1628.6 cm^{-1}, while other features were attributed to $\Delta K = \pm 1$ bands. These measurements provided a quantification of the monomer distortion that accompanies hydrogen bond formation. This measure is essential to incorporate into any water potential model.

In 2007, Nakayama et al. evaluated the interaction energy for water dimers by measuring pressure broadening coefficients of the $\nu_1 + \nu_3$ vibrational combination band of water monomers in the region 1.34–1.44 μm [46]. Various buffer gases, including inert gases (He, Ne, Ar, Kr and Xe) and N_2 and O_2 at varying pressures (60–500 Torr) were used with a constant partial pressure of water (0.04 Torr). Permenter–Seaver's energy transfer model [47] based on pressure broadening coefficients was used to evaluate the interaction energy for water dimers. The extracted experimental value (3.24 ± 0.95 kcal/mol) was smaller than some recent experimental values. Consideration of a structure averaged over different orientations of two colliding water molecules at 298 K rather than the dimer equilibrium geometry was proposed to account for the above discrepancy.

In 2008, Vigasin et al. measured the contribution of water dimers to the O—H stretching fundamental band profile of pure water vapor [48]. The spectra were recorded for 650 K and 673 K isotherms with 2 cm^{-1} spectral resolution. They were able to show that a simple monomer-dimer model gives an excellent fit for the O—H stretching spectral profile of water vapor up to a density of 0.04×10^{-3} kg/m^3. Vigasin subsequently rationalized the partial contributions of 'true bound' and 'metastable' dimer absorptions in the O—H stretching fundamental region of pressurized water vapor [49]. The experimental spectra were taken from the work of Jin and co-workers [48]. It was shown that 'metastable' water dimer absorption played a significant role in the temperature region from 573 to 773 K, compared to contributions from 'true bound' dimers. The experimental observations of Jin and co-workers were reanalyzed very recently by Tretyakov and Makarov using their newly developed model, which was based on high resolution monomer spectra and with the frequencies and intensities of rovibrational bands of the dimer and trimer derived from cold molecular beam experiments [50]. It was shown that the developed model yields a good fit to the O—H stretching fundamental band of high temperature (650 K) water vapor for densities up to 0.05 g/cm^3. The extracted value for the dimer equilibrium constant (K_d) 0.87×10^{-3} atm^{-1}, was in accord with the values obtained by some other groups [51].

Moudens et al. recorded FTIR spectra of water clusters up to pentamer in a planar slit jet expansion of Ar–water mixtures [52]. Clear signatures of free and hydrogen bonded O—H vibrations were observed for all the clusters. The peak position of the hydrogen bonded O—H stretching infrared frequency at 3601 cm^{-1} was consistent with previous experiments.

In 2011, Reisler and co-workers determined an accurate value of the bond dissociation energy (D_0) of the water dimer using velocity map imaging (VMI) and resonance enhanced multiphoton ionization (REMPI) [53]. The D_0 value (1105 ± 10 cm^{-1}) was in excellent agreement with the D_0 (1103 ± 4 cm^{-1}) value estimated by Shank et al. [54] utilizing a modified full-dimensional potential energy surface in association with CCSD(T)/aug-ccpVTZ theory and diffusion Monte Carlo calculations. In the subsequent year, Reisler and co-workers reported the bond dissociation energy D_0 for $(D_2O)_2$ using 2 + 1 REMPI and VMI techniques [55]. The obtained D_0 value for $(D_2O)_2$, 1244 ± 10 cm^{-1}, was in excellent agreement with the theoretical prediction (1244 ± 5 cm^{-1}) of Czakó et al. [56]. Experiment in combination with quasi-classical trajectory (QCT) calculation based on the HBB2 potential energy surface predicts (0 0 0) + (0 1 0) as the dominant dissociation channel for $(D_2O)_2$, wherein one quanta of the fragment bending mode is excited. Here

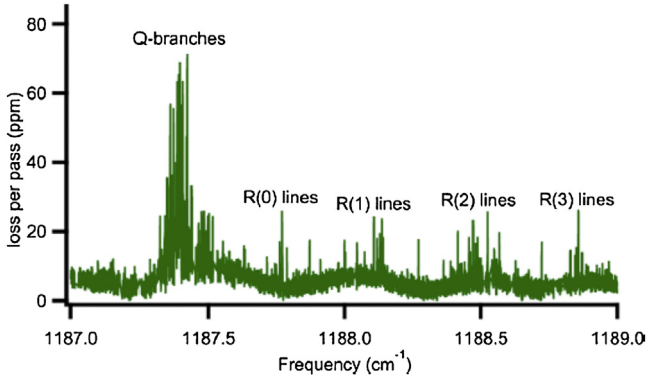

Figure 6. The bending vibration of $(D_2O)_2$. The infrared cavity ringdown spectrum for the K_a 1 ← 0 transitions of the hydrogen bond donor bending mode in an argon supersonic expansion. Transitions were determined to have originated from $A_1^+/E^+/B_1^+$ tunneling levels based on the strength of the transitions.
Reproduced with permission form Ref. [57].

(0 0 0) refers to the vibrational ground state and (0 1 0) refers to the first excited bending state following the notation developed in Ref. 10 of the above letter. The minor channel yielded highly rotationally excited fragments in their ground vibrational state.

Rotationally resolved spectra of the bending mode of $(D_2O)_2$ were reported by Stewart and McCall in 2013, complementing the corresponding $(H_2O)_2$ results of Paul et al. [45]. They used a supersonic jet expansion in combination with a quantum cascade laser-based cavity ringdown spectroscopy technique [57]. Two main bands appearing at 1187 and 1195 cm^{-1} were assigned to $K_a = 1 \leftarrow 0$ and $K_a = 2 \leftarrow 1$ subbands of the donor bending mode. They concluded that these two main features arose from overlapping Q branches of multiple tunneling states, wherein each Q branch is followed by an R branch with a regular 0.36 cm^{-1} separation between two consecutive R branches. This separation is almost twice the known B (0.1812) rotational constant for $(D_2O)_2$. Additionally, the assignment of two $\Delta K_a = 1$ bands was confirmed by the separation of $(2(A'\text{-}B') = 8$ $cm^{-1})$ for $(D_2O)_2$ dimer. The estimated band center at 1182.2 cm^{-1} yielded an excellent agreement (within 1 cm^{-1}) with the theoretical value from Wang et al.'s MULTIMODE calculation [58]. Figure 6 shows the K_a 1 ← 0 spectrum obtained by Stewart et al. and the assigned Q and R branches.

Földes et al. very recently (2014) reported rotationally resolved spectra of the H_2O dimer $2\nu_{OH}$ (overtone) band in the spectral region 7229–7262 cm^{-1} [59]. This new report helps to refine the previous assignment of Nizkorodov et al. [60]. In their vibrationally mediated laser dissociation spectroscopy experiment, Nizkorodov et al. used a tunable (7100–7300 cm^{-1}) near-infrared pump laser followed by ArF photolysis with a 0–1000 ns time delay from the pump beam. The photolysis beam dissociates a fraction of the vibrationally excited water molecules, and finally, a probe laser fixed at the $A^2X \leftarrow X^2\Pi$ $v = 1 \leftarrow 0$ band of OH with a time delay of 20 ns from the photolysis beam was used to probe the fluorescence of OH.

The measured spectrum is shown in Figure 7. Four bands appearing at 7193, 7240, 7249.8 and 7282 cm^{-1} were assigned to $(H_2O)_2$ [60]. The 7193 cm^{-1} band was assigned to the $|02\rangle_a{}^+/|1\rangle_f|1\rangle_b$ mode, where *a*, *f* and *b* stand for proton acceptor, free proton donor, and bound proton donor OH stretches, respectively. A slow scan over this region revealed a rotationally resolved structure. The 7240 and 7249.8 cm^{-1} bands were assigned to the $|2\rangle_f|0\rangle_b$ mode. The band appearing at 7282 cm^{-1} remained unassigned. Földes et al. observed eight broad features using Fourier transform, tunable diode and quadrupole mass spectrometers coupled with supersonic expansions [59]. Two weak bands appearing at 7233.9 and 7234.4 cm^{-1}, not listed in Nizkorodov et al.'s report, were assigned to other H_2O-containing clusters. The band at

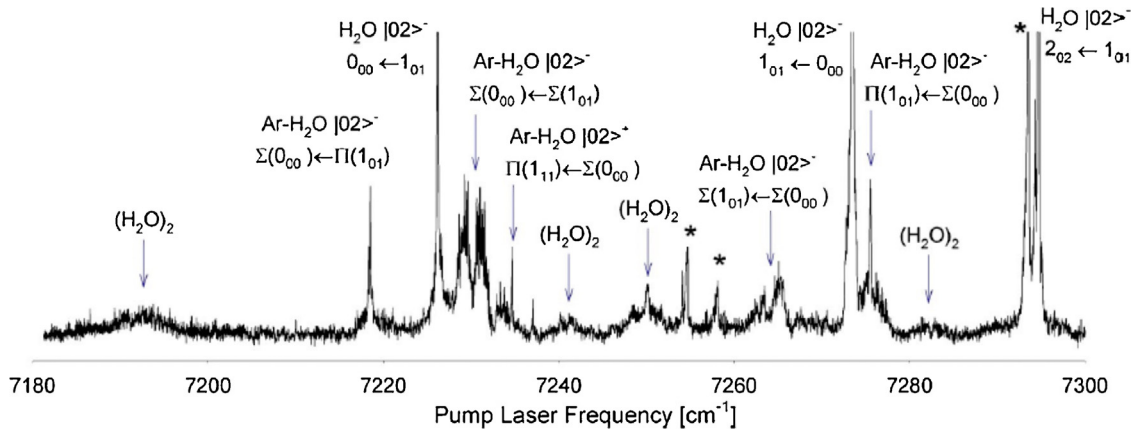

Figure 7. Dimer overtone spectra measured by vibrationally mediated laser photolysis. With permission from Ref. [47]. The spectra were obtained by tuning the probe pulse to the $^2\Pi_{3/2}{}^-$ state of OH(v = 0) while the pump laser was scanned in frequency. As indicated by the labels, the peaks result from water monomers and dimers as well as Ar–water dimers.

7256.5 cm^{-1} was previously assigned to Ar–H_2O. On the other hand, a sharp Q branch accompanied by R and P branches was observed and assigned to $(H_2O)_2$. This high energy feature overlapped with H_2O-rare gas lines that were confirmed from spectral shifts using different rare gases (Ar, Kr and Ne). They observed nine equally spaced R lines and five equally spaced P lines. The value of the dimer rotational constant (B + C)/2 for excited state was determined by fitting the experimental spectrum.

5. Water vapor continuum absorption: recent studies

Water vapor continuum absorption in the near-infrared region under different temperature and pressure conditions has been reported in the literature by several goups [61–65]. The definition of the continuum is an absorption whose cross section depends on the pressure of water vapor (self) and the buffer gas (foreign). A possible explanation for this continuum absorption is the presence of water clusters, particularly the dimer [61]. Near-infrared (5000–5600 cm^{-1}) pure water vapor absorption spectra were recorded at various pressures (98 and 20 kPa), temperatures (297 K, 299 K and 342 K) and path lengths (29 cm, 128 cm and 9.7 m) by Newnham and co-workers [66]. The measured laboratory spectral features match quite well with the atmospheric water vapor continuum spectra in the region of 5000–5500 cm^{-1}. This article provides an interesting description of the look at the role of the water dimers in the atmosphere. However, it should be noted that, their measured features could also be attributed to higher-order clusters because of higher water vapor pressure dependence.

Ravishankara and co-workers measured the water vapor absorption cross-section at different N_2 pressures (500–850 Torr) in the region of 10500–10800 cm^{-1} using cavity ringdown spectroscopy [61]. The measured line strength for several lines around 10,604 cm^{-1} yielded a good match with the HITRAN values. On the other hand, the overall absorption for the entire region appeared larger than the database value. Baranov and Lafferty measured water vapor continuum absorption in the spectral range of 2.88–5.18 μm under different temperature (311–363 K) and pressure (21–259 Torr) conditions using a FTIR Spectrometer [62]. The absorption coefficient at 5 μm was in good agreement with the results from the MTCKD continuum model. The MTCKD model is a semi-empirical computer simulation that computes the entire water continuum spectra and takes into account the effect of different gas species on the water lines [67]. In the self-continuum absorption near 3 μm, a distinct feature appearing at 3200 cm^{-1} was assigned to an overtone of a water dimer O—H—O bending vibration. The absorption coefficient of this bending vibration matches well with previously reported data taken at 351 K, this results indicates a significant contribution of the water dimer in that spectral region. The MTCKD_2.5 result yielded best agreement with the experimental data at 326 K, however significant deviations were observed at 311 K and 352 K. Unfortunately, this implies that neither the MTCKD nor the updated MTCKD_2.5 model can reliably predict the temperature dependence of the strong absorption coefficients [61]. This model contains an exponential dependence of the continuum absorption coefficient on temperature, while the observed dependence is much stronger than exponential. Figure 8 shows a comparison of predicted continuum absorptions from the different MTCKD versions along with a simulated dimer spectrum.

In 2011, Ptashink, Shine, and Vigasin critically reviewed recent work on water vapor continuum absorption and proposed a model that can explain both the wavelength and temperature dependences of continuum absorption [62]. The model, based on ab initio theoretical calculations and high-precision laboratory measurements, can distinguish the contributions of true bound dimers, quasi-bound dimers and free-pair collisions of water monomers to the continuum absorption. Contributions from quasi-bound dimers and true bound dimers based on VPT2 calculations were proposed to explain the laboratory measured continuum absorption in the near-IR region. The temperature dependence in the 8–12 μm range is explained by separation of true and quasi-bound dimer absorptions.

The observed larger continuum absorption compared to the MTCKD model results is attributed to possible dimer contributions in some definite near-IR windows. In 2013, Ptashink et al. reported self-continuum absorption in the spectral range of 1300–8000 cm^{-1} within the 289–318 K temperature range using a multipass cell of path length of 612 m and high resolution (0.03 cm^{-1}) Fourier Transform Spectrometry (FTS) as the probe [64]. They report self-continuum absorption at room temperature in the 6200 cm^{-1} (1.6 μm) frequency range. The self-continuum absorption in 4 μm (2700 cm^{-1}) and 2.1 μm (4000 cm^{-1}) region yielded a good agreement with the experimental result of Baranov [63] and Ptashink [68]. On the other hand, a discrepancy was found with the MTCKD results, indicating that the latter underestimates the experimental measurement, possibly due to the absence of dimer absorption in the model. Mondelain et al., in the same year investigated water vapor continuum absorption at room temperature in the 1.6 μm range using cavity ringdown spectroscopy [65]. The absorption coefficient was determined for the frequency range of 5875–6450 cm^{-1} with a varying pressure up to 12 Torr. The minimum absorption in this window was found at 6300 cm^{-1}. Pressure dependence of the absorption coefficient fit well to a

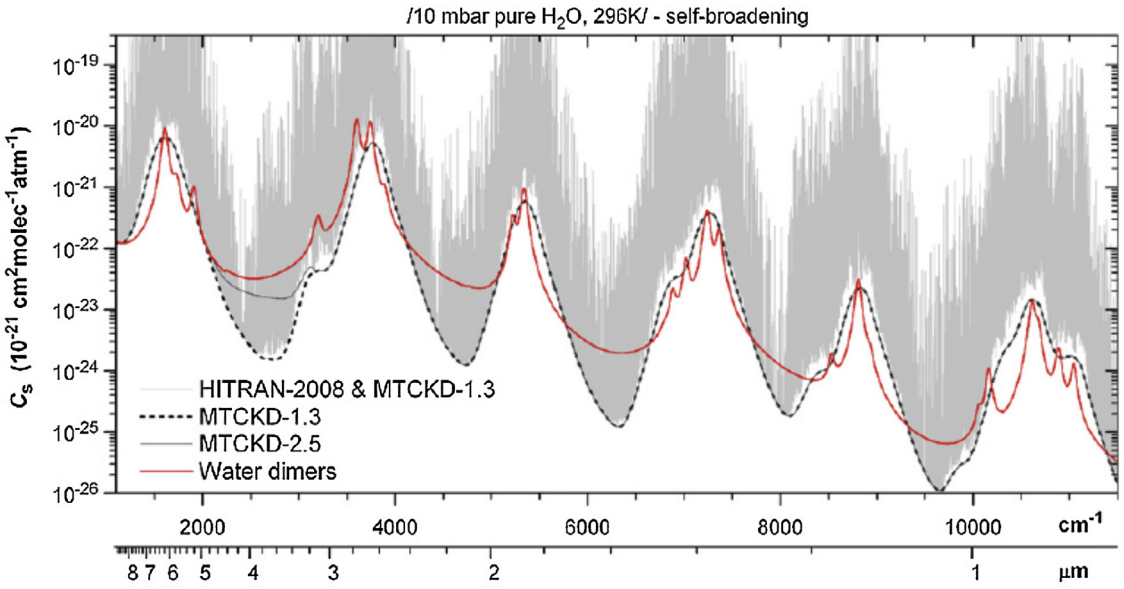

Figure 8. The near-IR water continuum. The figure displays the water continuum absorption for each MTCKD version along with a simulation of the water dimer absorbance in the same spectral region.
Reproduced with permission from Ref. [62].

second order polynomial, rather than showing purely quadratic dependence. This discrepancy was accounted for as water adsorption on the mirror surface, the first order term accounts for this adsorption [65]. The experimental self continuum absorption cross section (3×10^{-25} to 3×10^{-24} cm^2 $molecule^{-1}$ atm^{-1}) yielded a good agreement with the MTCKD_2.5 model, but disagreed with the Fourier transform spectroscopy measurements of Ptashink et al. [64], which yielded up to 2 orders of magnitude higher cross sections compared to Mondelain's measurements. Some possible explanations for this contrast are outlined in Mondelain's conclusion [65], but the question remains open.

6. Water dimers in exotic environments

The observation of small water clusters ($(H_2O)_n$ $n = 2, 3, 4$) in liquid helium droplets at very low temperatures (0.4 K) was first made in 1996 by Fröchtenicht et al. [69]. A small red shift (3.6 cm^{-1}) was observed for the dimer hydrogen bonded O—H stretching fundamental ($\nu_{O-H} = 3597.4$ cm^{-1} in He droplets), compared to the gas phase frequency. This red shift was attributed to the interaction with the solvent helium molecules, although the effect of this interaction on other O—H stretching modes of water dimer was negligible. The most striking feature was the narrowing of the dimer bands in liquid helium relative to gas phase spectra, which was thought to result from the very low temperature environment. Nauta et al. observed a linear dimer structure in liquid helium droplets, whereas cyclic structures were observed for trimer through hexamer [70]. Recently, rotationally resolved IR spectra were reported for mixed water dimers ($HDO\cdots H_2O$, $HDO\cdots HDO$ and $HDO\cdots D_2O$) embedded in liquid helium by Havenith and co-workers [71]. The covered spectral region included the O–D stretch (2650–2660 cm^{-1}) and symmetric stretch vibrations of acceptor (2725–2740 cm^{-1}) molecules. An observed increase in the linewidth was attributed to the intervibrational relaxation, which occurred due to the coupling between rovibrational levels. The observed ground state acceptor switching splitting for $HDO\cdots DOH$ was determined to be 5.68 cm^{-1}.

This technique provides a unique avenue to studying narrowed bands of the water dimer, and helps to elucidate the dynamical behavior of the dimer in this low temperature environment. Studying the tunneling motion in LHe droplets offers the advantage of avoiding the technical difficulties of supersonic molecular beams.

Infrared absorption spectra of water in CCl_4 solution was first recorded by Borst et al. [72]. Subsequently, molecular dynamics studies of monomeric water in CCl_4 were reported by Danten et al. [73]. Both of these studies were focused on monomeric structure and water–solvent interactions. In 2009, IR absorption spectra of both monomeric and dimeric water in CCl_4 solution were recorded by Nicolaisen in the spectral range of 3100–4200 cm^{-1} [74]. A new broad feature was observed at 3804 cm^{-1} that was assigned as a combination of an *intra*molecular OH stretching mode and an intermolecular vibration. However, the author recognizes that this assignment may be incorrect and the origin of the observed band is still an open question. The other measured dimer bands were consistent with the inert matrix and molecular beam results. After subtraction of monomer features from the entire absorption spectra, Nicolaisen concluded that the dimer contributes only 6% to the total absorption spectrum. Intensity enhancement was observed for both monomer and dimer due to water-solvent interactions.

7. Terahertz vibration–rotation tunneling (VRT) spectroscopy of the water dimer

The first terahertz (far-infrared) spectrum of the gaseous water dimer was observed near 22 cm^{-1} for $(H_2O)_2$ by Busarow et al. in 1989 using the Berkeley-tunable far-IR laser spectrometer coupled with a planar supersonic jet [75]. This work was contemporary with the microwave study of $(H_2O)_2$ published by Coudert et al., which reported a-type ($\Delta K = 0$) transitions and sampled one low frequency tunneling motion (donor-acceptor tunneling) of the vibrational ground state. Busarow et al. observed 350 transitions in the frequency range of 510–835 GHz range, and assigned 56 of them to a perpendicular band originating from the lower acceptor tunneling level of $K = 1$ to the lower acceptor tunneling level of $K = 2$. The first high resolution intermolecular vibrational spectrum of a water dimer[$(D_2O)_2$]was reported by Pugliano et al. in 1992 for a transition near 2.5 THz (84 cm^{-1}) [76]. The intermolecular vibration was assigned to the ν_8 mode (acceptor wag), which is associated with large amplitude motion of the hydrogen bond acceptor. The

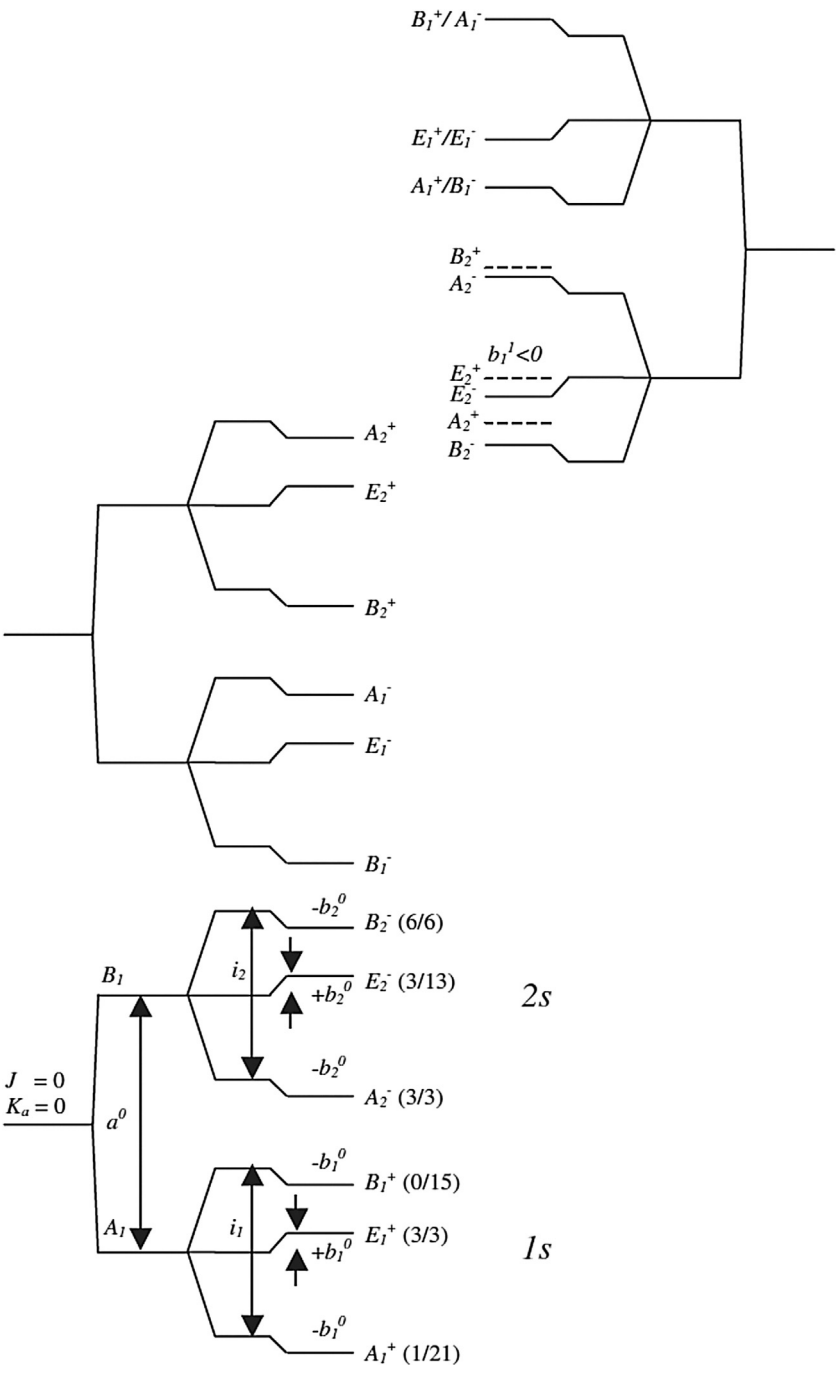

Figure 9. VRT energy level diagram for the water dimer. The levels are label based on their irreducible representation in the CNPI G_{16} group. The level diagrams on the LHS represent $K=0$ levels for $J=0.1$ while the RHS shows the diagram for $K=1$, $J=1$. Tunneling splittings are shown and labeled as: acceptor switching $=a^0$, interchange tunneling $=i_{1/2}$,and bifurcation tunneling $=b^0_{1/2}$. Numbers in parenthesis show the spin statistic weight for each level in H_2O and D_2O respectively. Each J, K level is divided into a set of two triplets, which are referred to as '1s', for the lower energy triplet, and '2s', for the higher energy triplet (in the case of the lowest energy state). Additionally, the $K=1$ levels show the effect of Coriolis coupling between the 2's of the J, $K=0$ level and the 2's of the J, $K=1$ level.

splitting due to donor tunneling increased from the ground state value of 6 MHz to the excited state value of 163 MHz, attributed to a reduction in tunneling barrier height in the excited state. In a subsequent letter, Pugliano et al. measured 230 transitions near 82.6 cm^{-1} and assigned them to 12 vibration-rotation-tunneling (VRT) sub-bands originating from lower $K_a=0$ to upper $K_a=0$ or 1 levels of $(D_2O)_2$ ν_8 acceptor bending motion [77]. In 1999, Fellers et al. determined a detailed polarizable water potential based on Stone's ab initio ASP models [78,79], fitting a small subset(4 or 6) of the total of 76 parameters to extensive water dimer data from microwave, terahertz and mid-IR spectra [80,81]. Braly et al. in 2000 reported four intermolecular vibrations of $(D_2O)_2$ comprising 731 transitions in the frequency region of 65–104 cm^{-1} [82]. The four intermolecular vibrations were assigned as donor torsion (ν_{12} mode) near 65 cm^{-1}, acceptor wag (ν_8 mode) near 83 cm^{-1}, acceptor twist (ν_{11} mode) near 90 cm^{-1} and in-plane bend (ν_6 mode) near 104 cm^{-1}. Later that same year, Braly et al. reported four intermolecular vibrations for $(H_2O)_2$ in the frequency range of 87 and 108 cm^{-1} comprising a total of 362 transitions [83]. The acceptor wag (ν_8 mode) motion was assigned to a feature observed near 102.1 cm^{-1}. Acceptor twist (ν_{11} mode) vibration was observed near 108 cm^{-1} and a 103.1 cm^{-1} band was assigned as

the in-plane bend (ν_6 mode) vibration of $(H_2O)_2$. These two articles by Braly et al. provide a fairly complete overview of both $(H_2O)_2$ and $(D_2O)_2$ intermolecular bend(torsion) and stretch vibrations, including great deal of VRT data. In 2002, Goldman et al. [84] and Leforestier et al. [85] determined new water potential surfaces by fitting the experimental VRT data for the dimer provided by the Saykally group. Details will be discussed in later section. Subsequently, Keutsch et al. reported high frequency terahertz spectra between 140.5 cm^{-1} and 145.5 cm^{-1} [86]. The spectrum was assigned to both the hydrogen bond translational mode and donor torsion overtone mode in which 64 new K-subbands were observed for $(H_2O)_2$ and 16 new K-subbands were assigned to $(D_2O)_2$. Both the observed interchange splitting and bifurcation tunneling splitting in the excited state were respectively three and two times larger than the ground state splittings, again due to a reduced tunneling barrier in the excited state. Keutsch et al. later reported rotation-tunneling spectra of both $(H_2O)_2$ and $(D_2O)_2$ with higher value of K, viz. $K = 0–3$ and $K = 0–4$ for H_2O and D_2O, respectively, in the region of 70–80 cm^{-1} [87]. Experimentally determined molecular constants and tunneling splittings were compared with different model potential energy surfaces (Figure 9).

In 2007, Harker et al. combined the values of experimentally determined rotational constants and tunneling splittings to predict the fingerprint of weakly allowed $E_2 \leftrightarrow E_1$ transitions and the transition frequencies of both $(H_2O)_2$ and $(D_2O)_2$ dimer [88]. A global fitting program with a prolate rotor energy expression was used, wherein a total of 391 $(D_2O)_2$ lines and 343 $(H_2O)_2$ lines were fit and analyzed separately. The analysis yielded expressions for the ground and excited state acceptor switching (AS) splitting as a combination of transition between 1s and 2s triplets. The expressions are as follows:

$$AS^{(0)} + AS^{(1)} = \nu_{1s}^{(0,1)} - \nu_{2s}^{(0,1)}.$$

$$AS^{(2)} - AS^{(1)} = \nu_{1s}^{(0,2)} - \nu_{2s}^{(0,1)} - \nu_{1s}^{(0,1)} - \nu_{2s}^{(0,1)}.$$

These equations are helpful to precisely determine an unknown AS splitting from a previously known AS value, as various K_a triplets are linked by c-type transitions. Using ground state acceptor switching splitting values (53,000 MHz for $(D_2O)_2$ and 279,650 MHz for $((H_2O)_2)$ along with the accurate rotational constants, they predicted the frequencies of $E_2 \leftrightarrow E_1$ transitions.

Harker et al. next reported the measurement of four new subbands of the hydrogen bond stretch (S) [89]. The Berkeley THz VRT spectrometer was extended to higher frequencies (4 THz) by using two 70 μm (4251.6736 GHz) CH_3OH and 72 μm (4158.9158 GHz) $^{13}CH_3OH$ FIR lasers and a KVARZ millimeter synthesizer which covered frequencies from 53 to 118 GHz. Four new donor S subbands were identified, and the donor torsion overtone $(DT)^2$ and hydrogen bond stretch (S) subbands observed by Keutsch et al. [71] were augmented by these authors. Harker et al. proposed reassignment of the 4261 GHz band to $K_a = 1(E_1) \leftarrow 1(E_2)$, whereas the previous assignment was as the $(DT)^2$ $K_a = 0 \leftarrow 1_{(lower)}$ or E_2 $K_a = 1 \leftarrow 1_{(lower)}$ transition. The 4295 GHz Q-branch was assigned to the $(DT)^2$ E_1 $K_a = 1 \leftarrow 0$ subband.

To date Terahertz VRT spectroscopy of the water dimer has provided the most accurate determination of the rotational constants. The assigned VRT transitions serve a crucial test for any new potential model, as the model must be capable of reproducing the observed transitions. In the future, as the absent libration modes of the dimer are measured, inversion of the assigned energy levels provide the promise of determining an accurate potential for the two body interaction. These modes remain essential fro determination of the role of hydrogen bonds in the bulk water medium.

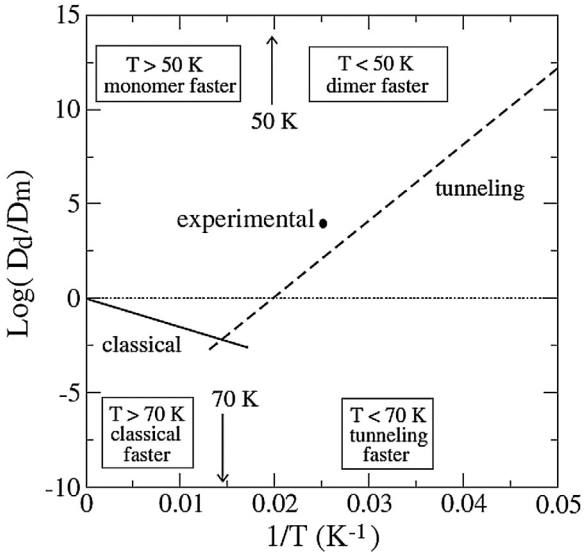

Figure 10. Temperature dependent dimer diffusion rates. Comparison of rates for water monomers and dimers with respect to temperature on Pd{1 1 1}. $D_{d/m}$ represents the rate of diffusion for the dimer or monomer respectively.

8. Water dimer diffusion on metal surfaces

Several groups have studied cluster formation and interactions of water on metal surfaces using several spectroscopic techniques (viz. high-resolution electron energy loss spectroscopy [90,91] infrared spectroscopy [92,93] and helium atom scattering [94]). Mitsui et al. (2002) reported water adsorption, aggregation and diffusion on a Pd(1 1 1) surface using STM [95]. Clusters ranging from dimer through pentamer were observed. A rapid diffusion of water dimers (residence time of 120 ms on a site) was observed. A lower limit of the diffusion constant $D_2 \geq 50\,Å^2\,s^{-1}$ for water dimer on a Pd(1 1 1) surface was extracted from STM movies at 40 K. This high mobility (ca. 10^4 times larger than other water clusters) of water dimers was attributed to the strong hydrogen bond between the water molecules and a mismatch between the dimer O—O (2.96 ± 0.05 Å from gas phase experiments) bond length and the Pd(1 1 1) lattice constant (2.75 Å). Later, Ranea et al. presented a novel mechanism for the diffusion of water dimers on Pd(1 1 1) surface based on density functional theory [96].

The DFT calculation predicts that the adsorbed water molecule lies in a plane parallel to the substrate surface. The calculated adsorption energy is 0.33 eV and the O—O distance is 2.74 Å, which is 0.2 Å shorter then the to gas phase water dimer equilibrium O—O distance. Ranea et al. adopted the mechanism of donor-acceptor interchange, described in Saykally group work [81], which nicely explains the large value of the diffusion constant experimentally observed by Mitsui et al. Figure 10 shows the newly established domains of diffusion determined by Ranea et al., in the quantum regime (less than 70 K) tunneling was found to rearrange the H-bond network and account for the change in diffusion. Kumagai et al. reported direct observation of hydrogen bond exchange in water dimers on a Cu(1 1 0) surface using STM [97]. $(H_2O)_2$ dimers on this surface at 6K show preferred stability relative to water monomers, and a ~0.2 V voltage pulse was required to dissociate this dimer. The $(D_2O)_2$ dimer, on the other hand, appeared stationary compared to $(H_2O)_2$. A temporal profile of the interchange motion was obtained by recording tunneling current with the STM tip fixed on the $(H_2O)_2$ dimer. A jump in tunneling current was observed between two consecutive interchange events. The obtained interchange rate was $(6.0 \pm 0.6) \times 10^1\,s^{-1}$ for $(H_2O)_2$ and $(1.0 \pm 0.1)\,s^{-1}$ for $(D_2O)_2$. This seven orders-of-magnitude

reduction in interchange rate compared to gas phase results (interchange rate$\sim 10^9\ s^{-1}$ for $(H_2O)_2$) was attributed to the tenfold increased barrier height on the surface(23 kJ/mol on Cu(1 1 0) compared to 2.48 kJ/mol in gas phase [81]).

9. Development of water dimer potential surfaces from experiment

The great interest in the water dimer emanates largely from its central role in the development of an ultimate water potential model. In this ultimate water potential, the two-body terms are completely analogous to the dimer potential, and provide quantitative insight into the most unique feature of water – the hydrogen bond. Current issues regarding the development of improved bulk water models apply even to the dimer models, e.g. the number of interaction sites in the dimer complex, whether to use flexible or rigid monomers, and the proper inclusion of polarizability(induction) and dispersion. Researchers must address the tradeoff between accuracy and computational expediency. Regardless of the method, however, any potential model should suitably reproduce the spectroscopic results outlined within this review.

A logical starting point for the discussion of dimer potentials is Jorgensen et al.'s 1983 review of, the existing potential models, viz. BF, SPC, ST2, TIPS2, TIP3P, and TIP4P. Classical Monte Carlo simulations showed that these models gave good agreement with the experimental monomer geometry, but displayed poor accuracy for the dimer structure. For example, all these potential models predicted a hydrogen bond energy that was nearly twice the accepted value of 3.40 kcal/mol. Additionally, the oxygen-oxygen separation was consistently overestimated by about 10%. This review demonstrates that models with greater number of interaction sites, generally give a more accurate representation of the dimer geometry [98]. Later that same year, Reimers and Watts published a study wherein deformable monomers were used in a model for water clusters up to tetramers. Using this framework, the authors developed a semi-empirical model for the intermolecular vibrations of the dimer. The calculated vibrational frequencies all overestimated the observed bands from VRT and matrix isolation experiments [99].

Stone and coworkers developed an ab initio potential for bulk water using known monomer properties and perturbation theory calculations for the dimer. Long range interactions were modeled using a distributed multipole method. The developed model, called ASP, did extremely well in reproducing the monomer and dimer geometries, although the model was constrained to fit a linear geometry for the dimer which will impact the prediction of dimer energies in other configurations. Nevertheless, the calculated geometry produced the best-to-date agreement with the experimental structure. The calculated binding energy of the dimer was underestimated compared to other potential models, but still fell in the range of the experimental uncertainty. One drawback to this model is that calculations of the second virial coefficient indicated that, especially at lower temperatures, the potential overpredicted the depth of the global minimum [78]. The ASP model was also used to calculate the tunneling splittings of the water dimer with limited success. The real power of the ASP model was that the water potential was constructed as a sum of the different energy components (one-body, two-body, etc.) which allows the model to be improved as more experimental data become available. Several years later, explicit higher order cluster terms were included in the model, leading to improvements in the dimer binding energy. That letter also reports predictions for the contribution of higher order terms to the overall potential model [100].

The key limitation of the Stone ASP model was the absence of the electron–electron correlation energies. This can be accounted for by applying symmetry adapted perturbation theory (SAPT), as outlined by Jeziorski et al. [101]. Applying this model to the water dimer, extremely accurate calculations of the interaction energy were obtained, viz. 4.7 ± 0.2 kcal/mol, compared to the accepted value of 4.7 ± 0.1 kcal/mol obtained from large basis set, supermolecular calculations.

An alternative route to determining an universal water potential is direct inversion of spectroscopic results. In 2002, Goldman et al. presented two 6D, polarizable dimer potential models obtained from fitting of microwave, VRT, and mid-IR cavity ringdown data along with the ab initio parameters in the ASP model. The data were fit by varying a small subset of the 72 parameters of the ASP model and resulted in excellent agreement of binding energies and second virial coefficients [84]. Furthermore, the new models were able to reproduce experimental VRT spectra, and therefore included estimates of the three tunneling pathways of the water dimer. These potentials, VRT(ASP)II and VRT(ASP)III, predicted intermolecular vibration frequencies and tunneling splittings shown in Tables 1 and 2.

It can be seen that the results for $(D_2O)_2$ are better represented by the new models, whereas results for $(H_2O)_2$ are only marginally better than from SAPT. This work was extended later that same year to include *flexible* monomers in a version of Clementi's MCY potential, thus making the calculation span 12D ('full-dimensional'), this new model was named VRT(MCY-5f). The full-dimensional calculation was achieved by adiabatic separation of the slow, intermolecular, and fast, *intra*monomeric, modes, which allows recasting the calculation to a parametric 6D form, thus allowing simpler computation while still considering monomer flexibility [85]. Better agreement with spectroscopic properties was obtained with the simpler but fully flexible VRT(MCY-5f) model for both inter- and intra-molecular vibrations of the water dimer than was obtained with the more elaborate but rigid VRT(ASP)III. As a result, the predicted VRT spectra of the dimer were in excellent agreement with the experimental data existing at the time.

Very soon after this, Keutsch et al. published a complete characterization of the dimer grounds state for both $(D_2O)_2$ and $(H_2O)_2$. In that letter, an explicit comparison is made between VRT(ASP)III, SAPT, and VRT(MCY-5f) [87], and the interested reader is directed to that letter for the details, viz. Tables 5, 6, 7, and 8. As all three potential models give good agreement with experimental spectroscopic properties, a comparison of the tunneling splittings is enlightening. For the $(H_2O)_2$ complex, the acceptor tunneling was found to be best reproduced by the VRT(MCY-5f) model, which yielded agreement to within of 1% of the experimental value. However, for both interchange and bifurcation tunneling, the SAPT model was superior. However, it is important to note that at higher rotational quantum number K, values the VRT(MCY-5f) model better reproduce the interchange splittings. The overall results of the study concluded that the SAPT model was in best agreement with the experimental results, which can be rationalized by recalling that the model was 'tuned' to the $(H_2O)_2$ data which could explain the slight deviations that are observed in the $(D_2O)_2$ results.

Very recently, realization of a full-dimensional, flexible potential that includes polarizability has come to fruition. Leforestier et al. presented new results using a rigid water pair potential calculated at the coupled cluster level of theory, then adapted into a flexible pair potential. A decoupling of the fast and slow monomeric modes, similar to that used to develop the VRT(MCY-5f) model, was again employed to simplify the calculation [102]. This new model, CCpol-8sf, displays extreme accuracy with respect to VRT energy levels and precisely predicted the binding energy of the water dimer. The geometry of the dimer is also predicted to a greater degree of accuracy then in the SAPT model. Details of the calculation are presented in Ref. [101], and no elaboration will be attempted in this review. However, the results of this potential model are very

Table 1
Comparison of potential models for $(H_2O)_2$ *inter*molecular vibrations.

	Ground state				Acceptor wag (ν_8)			
	VRT(ASP-W)II	VRT(ASP-W)III	SAPT5st	Experiment	VRT(ASP-W)II	VRT(ASP-W)III	SAPT5st	Experiment
Band Origin (1)	0.00	0.00	0.00	0.00	108.74	108.17	113.39	107.93
Band Origin (2)	11.86	10.67	11.18	11.18	99.50	99.93	110.00	97.71
Interchange (1)	0.60	0.36	0.72	0.75	2.44	1.14	2.60	2.95
Interchange (2)	0.59	0.39	0.65	0.65	−0.27	0.02	0.65	0.02
Acceptor Switching	11.86	10.67	11.18	11.18	−9.23	−8.24	−3.39	−10.20
	Donor torsion (ν_{12})				Acceptor twist (ν_{11})			
	VRT(ASP-W)II	VRT(ASP-W)III	SAPT5st	Experiment	VRT(ASP-W)II	VRT(ASP-W)III	SAPT5st	Experiment
Band Origin (1)	110.66	118.19	118.26	–	130.46	136.31	132.31	–
Band Origin (2)	69.76	73.28	64.52	64.44	106.55	121.02	120.97	120.19
Interchange (1)	4.12	1.54	3.05	1.11	0.70	2.40	4.99	–
Interchange (2)	1.33	0.397	1.72	2.54	6.84	4.92	10.36	9.39
Acceptor Switching	40.91	44.91	64.92	–	23.71	15.29	11.46	–
	In-plane bend (ν_6)				O—O stretch (ν_7)			
	VRT(ASP-W)II	VRT(ASP-W)III	SAPT5st	Experiment	VRT(ASP-W)II	VRT(ASP-W)III	SAPT5st	Experiment
Band Origin (1)	133.69	138.46	134.37	–	138.67	148.90	–	–
Band Origin (2)	150.83	152.65	148.22	∼103.1	178.42	186.12	–	142.44
Interchange (1)	7.88	0.452	8.25	–	1.81	2.47	–	–
Interchange (2)	2.33	0.519	0.56	–	20.05	8.49	–	1.88
Acceptor Switching	17.14	14.19	22.08	–	39.74	39.22	–	–

Table 2
Comparison of potential models for $(D_2O)_2$ *inter*molecular vibrations. A single asterisk indicates experimental data included in the VRT(ASP-W)II fit, and double asterisks indicate data included in the VRT(ASP-W)III fit.

	Ground state				Acceptor wag (ν_8)			
	VRT(ASP-W)II	VRT(ASP-W)III	SAPT5st	Experiment	VRT(ASP-W)II	VRT(ASP-W)III	SAPT5st	Experiment
Band Origin (1)	0.00	0.00	0.00	0.00	82.82	83.76	89.82	82.64**
Band Origin (2)	1.77	1.65	1.69	1.77*	80.98	82.83	95.03	84.40**
Interchange (1)	0.04	0.02	0.0393	0.04*	0.16	0.06	0.15	0.13*
Interchange (2)	0.04	0.02	0.0385	0.04*	0.07	0.04	0.23	0.11*
Acceptor Switching	1.77	1.65	1.69	1.77*	-1.83	-0.93	5.21	1.76
	Donor torsion (ν_{12})				Acceptor twist (ν_{11})			
	VRT(ASP-W)II	VRT(ASP-W)III	SAPT5st	Experiment	VRT(ASP-W)II	VRT(ASP-W)III	SAPT5st	Experiment
Band Origin (1)	74.74	78.50	76.26	75.38*	83.08	93.46	93.78	92.91**
Band Origin (2)	64.06	64.93	60.13	59.59**	74.35	88.62	91.98	90.37**
Interchange (1)	0.53	0.08	0.10	0.33*	0.12	0.24	0.8407	0.43
Interchange (2)	0.06	0.02	0.11	0.27	0.67	0.32	0.9965	0.44
Acceptor Switching	10.68	13.57	16.13	15.81	8.74	4.84	1.80	2.54
	In-plane bend (ν_6)				O-O stretch (ν_7)			
	VRT(ASP-W)II	VRT(ASP-W)III	SAPT5st	Experiment	VRT(ASP-W)II	VRT(ASP-W)III	SAPT5st	Experiment
Band Origin (1)	103.94	108.93	107.32	104.24*	130.03	149.41	144.44	–
Band Origin (2)	129.80	132.86	140.50	–	137.62	153.71	150.88	–
Interchange (1)	0.38	0.05	0.6905	0.78*	5.64	0.13	1.399	–
Interchange (2)	3.97	0.27	0.1312	–	1.94	5.23	0.0175	–
Acceptor Switching	25.86	23.93	33.19	–	7.60	4.30	6.44	–

Table 3
Comparison of MB-pol to other leading potential models. HBB2 is a model which incorporates flexible monomers into an *ab initio* model. Some inaccuracies exist as a result of missing experimental studies of particular bands.

			Experiment	HBB2	CCpol-8s/f	MB-pol		Experiment	HBB2	CCpol-8s/f	MB-pol
OO	-	(2)	153.62 (1.88)	148.57 (1.14)	149.63 (.23)	154.31 (2.41)	(1)		152.50 (1.12)	152.07 (1.48)	156.60 (2.71)
	-	(1)		145.00 (3.48)	143.20 (3.27)	149.44 (1.97)	(2)		150.52 (1.04)	153.54 (2.54)	152.69 (4.13)
AT	-	(1)		128.91 (0.74)	132.10 (1.48)	129.44 (0.24)	(1)		142.25 (4.33)	142.42 (4.04)	143.68 (4.87)
	-	(2)	120.19 (9.39)	121.01 (8.41)	117.50 (8.67)	119.07 (10.15)	(2)		136.24 (5.31)	136.52 (4.66)	137.04 (5.95)
AW	-	(2)	108.89 (0.002)	105.78 (0.03)	107.82 (0.10)	108.87 (0.13)	(2)	123.56 (3.41)	122.25 (2.48)	123.12 (3.16)	123.65 (3.83)
	-	(1)	107.93 (2.95)	105.35 (1.99)	109.23 (3.29)	108.38 (3.24)	(1)	109.98 (5.24)	108.95 (4.55)	108.28 (4.76)	109.65 (5.89)
DT	-	(1)		116.54 (4.84)	113.35 (5.91)	113.83 (5.61)	(2)		94.25 (2.66)	92.18 (3.34)	91.22 (3.47)
	-	(2)	64.52 (2.54)	67.18 (2.03)	61.33 (2.48)	61.31 (2.54)	(1)	87.75 (1.11)	89.55 (0.54)	86.37 (1.32)	85.63 (1.00)
GS	-	(2)	11.18 (0.65)	10.16 (0.60)	12.75 (0.61)	12.05 (0.69)	(1)	14.39 (0.70)	14.00 (0.64)	15.45 (0.67)	15.04 (0.77)
	-	(1)	0.00 (0.75)	0.00 (0.68)	0.00 (0.72)	0.00 (0.81)	(2)	11.66 (0.54)	11.50 (0.49)	12.36 (0.51)	12.18 (0.48)
				$K=0$						$K=1$	

satisfactory for predicting not only the band origins and redshifts of the intermolecular vibrations, but also the tunneling splittings. In the majority of cases, the CCpol-8sf potential agrees to within a percent or two with the experimentally determined VRT spectra. Further improvements have yielded the most accurate dimer potential model to date, published by Babin et al. [103]. This model, MB-pol, while computationally expensive, predicts spectroscopic properties and spectra for the dimer that are in nearly quantitative agreement. A direct comparison of this potential model with the next, most accurate, models is shown in Table 3.

In the future, potential models will continue to be improved by including experimental measurements of elusive intermolecular modes, such as the in-plane and out-of-plane librational modes and complete data for all isotopomers. While it seems imperative to include the full-dimensionality of the complex in terms of flexible monomers in additional to explicit polarizability terms, the computational expense of these models limits their usefulness for condensed phase simulations, they nevertheless serve as benchmarks for ongoing experimental and theoretical studies. Developing still more elegant, computationally efficient models would serve to greatly expand the possible applications.

10. Conclusions

The study of water clusters is driven by the quest for the 'ultimate' water model-a water potential surface that is capable of accurately predicting any property of the bulk forms and reproducing all experimental results. Such a model would have obvious applications in essentially any subject involving water. This level of understanding could definitively describe and predict the complex behavior of the most ubiquitous substance on the planet.

In the six decades since Pimentel and coworkers first observed the water dimer, remarkable advances in the understanding of this unique complex have been achieved. We now accept that the structure of the water dimer comprises a near-linear hydrogen bond between a donor and an acceptor, as shown in Figure 1. The results presented herein summarize the current understanding of the quantum structure and dynamics of the water dimer and the efforts toward determining an 'ultimate' twelve dimensional potential energy surface for the complex.

High-resolution spectroscopy experiments have determined the energy level structure for most of the dimer rotational and vibrational modes. The ground state has been completely characterized by microwave experiments in molecular beams, which establishes a firm starting point for future spectroscopic studies. In the mid-IR region, several techniques have been successful in measuring the *intra*molecular vibrations of the water dimer. From terahertz VRT spectroscopy experiments, most of the *inter*molecular modes of the dimer have been characterized. However, it is essential to note that the two librational modes for the dimer, the in-plane and out-of-plane bend, remain elusive. Matrix isolation experiments have provided good clues to their spectroscopic location, but until characterized by a high-resolution technique, this vital piece of the PES is missing. These librational motions are crucial to understanding the dynamics of hydrogen bond formation and breaking in the liquid, so continued efforts to observe them are urgently needed. The key limitation is the current lack of spectral coverage in the 200–700 cm^{-1} region. Development of new laser systems is thus essential to characterizing these librational modes.

While the MB-pol potential model described in the previous section represents a nearly complete dimer model, it still lacks information regarding the librational modes. Once measured and incorporated into such a model, the two-body part of the 'ultimate' potential will have been completed. The remaining task is then to determine the three-body and higher-order terms through a similarly detailed study of water trimers and larger clusters. Fortunately, many of the experimental techniques discussed within this review have also been applied to these larger clusters, and a considerable understanding of these systems has already been achieved. For example, the 21-dimensional VRT dynamics of the trimer have been addressed by sequentially more sophisticated calculations, and a full-dimensional model seems close at hand.

Acknowledgements

The Berkeley Terahertz spectroscopy effort is supported by the Experimental Physical Chemistry Division of the National Science Foundation under Grant No. 1300723.

References

[1] M. Van Thiel, E.D. Becker, G.C. Pimentel, J. Chem. Phys. 27 (1957) 486.
[2] A.J. Tursi, E.R. Nixon, J. Chem. Phys. 52 (1970) 1521.
[3] L. Fredin, B. Nelander, G. Ribbegard, Chem. Phys. Lett. 36 (1975) 375.
[4] L. Fredin, B. Nelander, G.J. Ribbegard, Chem. Phys. 66 (1977) 4065.
[5] R.M. Bentwood, A.J. Barnes, W.J. Orville-Thomas, J. Mol. Spectrosc. 84 (1980) 391.
[6] A. Engdahl, B.J. Nelander, Chem. Phys. 86 (1987) 1819.
[7] B.J. Nelander, Chem. Phys. 88 (1988) 5254.
[8] D. Forney, M.E. Jacox, W.E. Thompson, J. Mol. Spectrosc. 157 (1993) 479.
[9] J.P. Perchard, Chem. Phys. 266 (2001) 109.
[10] J. Perchard, Chem. Phys. 273 (2001) 217.
[11] Y. Bouteiller, J.P. Perchard, Chem. Phys. 305 (2004) 1.
[12] Y. Bouteiller, B. Tremblay, J.P. Perchard, Chem. Phys. 386 (2011) 29.
[13] J. Ceponkus, P. Uvdal, B.J. Nelander, Chem. Phys. 129 (2008) 194306.
[14] J. Ceponkus, B.J. Nelander, Phys. Chem. A 108 (2004) 6499.
[15] J. Ceponkus, P. Uvdal, B.J. Nelander, Phys. Chem. A 112 (2008) 3921.
[16] J. Ceponkus, P. Uvdal, B.J. Nelander, Chem. Phys. 133 (2010) 074301.
[17] J. Ceponkus, P. Uvdal, B.J. Nelander, Phys. Chem. A 115 (2011) 7921.
[18] R. Sliter, M. Gish, A.F. Vilesov, J. Phys. Chem. A 115 (2011) 9682.
[19] B. Tremblay, Y. Bouteiller, J.P. Perchard, Chem. Phys. 382 (2011) 15.
[20] J. Ceponkus, P. Uvdal, B.J. Nelander, Phys. Chem. A 116 (2012) 4842.
[21] J. Ceponkus, A. Engdahl, P. Uvdal, B. Nelander, Chem. Phys. Lett. 581 (2013) 1.
[22] T.R. Dyke, J.S. Muenter, J. Chem. Phys. 60 (1974) 2929.
[23] T.R.J. Dyke, Chem. Phys. 66 (1977) 492.
[24] T.R. Dyke, K.M. Mack, J.S. Muenter, J. Chem. Phys. 66 (1977) 498.
[25] J.A. Odutola, T.R. Dyke, J. Chem. Phys. 72 (1980) 5062.
[26] L.H. Coudert, F.J. Lovas, R.D. Suenram, J.T. Hougen, J. Chem. Phys. 87 (1987) 6290.
[27] J. Odutola, A.T. Hu, A.D. Prinslow, S.E. O'dell, T.R. Dyke, J. Chem. Phys. 88 (1988) 5352.
[28] G.T. Fraser, R.D. Suenram, L.H. Coudert, J. Chem. Phys. 90 (1989) 6077.
[29] E. Zwart, J.J. Meulen, W.L. Meerts, Chem. Phys. Lett. 173 (1990) 115.
[30] E. Zwart, J.J.T. Meulen, W.L. Meerts, J. Mol. Spectrosc. 147 (1991) 27.
[31] G.T. Fraser, F.J. Lovas, R.D. Suenram, E.N. Karyakin, A. Grushow, W. Burns, A.K.R. Leopold, J. Mol. Spectrosc. 181 (1997) 229.
[32] L.H. Coudert, W. Caminati, M. Schnell, J.-U. Grabow, J. Mol. Spectrosc. 242 (2007) 118.
[33] M. Tretyakov, E. Serov, M. Koshelev, V. Parshin, A. Krupnov, Phys. Rev. Lett. 110 (2013) 093001.
[34] R. Saykally, Physics (College Park, MD) 6 (2013) 22.
[35] T.A. Odintsova, M.Y. Tretyakov, A.F. Krupnov, C.J. Leforestier, Quant. Spectrosc. Radiat. Transf. 140 (2014) 75.
[36] F.N. Keutsch, J.D. Cruzan, R.J. Saykally, Chem. Rev. 103 (2003) 2533.
[37] M.F. Vernon, D.J. Krajnovich, H.S. Kwok, J.M. Lisy, Y.R. Shen, Y.T. Lee, J. Chem. Phys. 77 (1982) 47.
[38] R.H. Page, G.F. Jeremy, Y.R. Shen, Y.T. Lee, Chem. Phys. Lett. 106 (1984) 373.
[39] D.F. Coker, R.E. Miller, R.O. Watts, J. Chem. Phys. 82 (1985) 3554.
[40] J.R. Reimers, R.O. Watts, M.L. Klein, Chem. Phys. 64 (1982) 95.
[41] F. Huisken, M. Kaloudis, A.J. Kulcke, Chem. Phys. 104 (1996) 17.
[42] Z.S. Huang, R.E. Miller, J. Chem. Phys. 91 (1989) 6613.
[43] J.B. Paul, C.P. Collier, R.J. Saykally, J.J. Scherer, A.O. Keefe, J. Phys. Chem. A 101 (1997) 5211.
[44] J.B. Paul, R.A. Provencal, C. Chapo, A. Petterson, R.J. Saykally, J. Chem. Phys. 109 (1998) 10201.
[45] J.B. Paul, R.A. Provencal, C. Chapo, K. Roth, R. Casaes, R.J. Saykally, J. Phys. Chem. A 103 (1999) 2972.
[46] T. Nakayama, H. Fukuda, T. Kamikawa, Y. Sakamoto, A. Sugita, M. Kawasaki, T. Amano, H. Sato, S. Sakaki, I. Morino, G.J. Inoue, Chem. Phys. 127 (2007) 134302.
[47] H.-M. Lin, M. Seaver, K.Y. Tang, A.E.W. Knight, C.S. Parmenter, J. Chem. Phys. 70 (1979) 5442.
[48] A.A. Vigasin, Y. Jin, S. Ikawa, Mol. Phys. 106 (2008) 1155.
[49] A.A. Vigasin, Mol. Phys. 108 (2010) 2309.
[50] M.Y. Tretyakov, D.S. Makarov, J. Chem. Phys. 134 (2011) 084306.

[51] L.A. Curtiss, D.J. Frurip, M.J. Blander, Chem. Phys. 71 (1979) 2703.
[52] A. Moudens, R. Georges, M. Goubet, J. Makarewicz, S.E. Lokshtanov, A.A. Vigasin, J. Chem. Phys. 131 (2009) 204312.
[53] B.E. Rocher-Casterline, L.C. Ch'ng, A.K. Mollner, H.J. Reisler, Chem. Phys. 134 (2011) 211101.
[54] A. Shank, Y. Wang, A. Kaledin, B.J. Braams, J.M. Bowman, J. Chem. Phys. 130 (2009) 144314.
[55] L.C. Ch'ng, A.K. Samanta, G. Czako, J.M. Bowman, H.J. Reisler, Am. Chem. Soc. 134 (2012) 15430.
[56] G. Czakó, Y. Wang, J.M. Bowman, J. Chem. Phys. 135 (2011) 151102.
[57] J.T. Stewart, B.J. McCall, J. Phys. Chem. A 117 (2013) 13491.
[58] Y. Wang, S. Carter, B.J. Braams, J.M. Bowman, J. Chem. Phys. 128 (2008) 071101.
[59] T. Földes, T. Vanfleteren, M.J. Herman, Chem. Phys. 141 (2014) 111103.
[60] S.A. Nizkorodov, M. Ziemkiewicz, D.J. Nesbitt, A.E.W. Knight, J. Chem. Phys. 122 (2005) 194316.
[61] M. Aldener, S.S. Brown, H. Stark, J.S. Daniel, A.R. Ravishankara, J. Mol. Spectrosc. 232 (2005) 223.
[62] I.V. Ptashnik, K.P. Shine, A.A. Vigasin, J. Quant. Spectrosc. Radiat. Transf. 112 (2011) 1286.
[63] Y.I. Baranov, W.J. Lafferty, J. Quant. Spectrosc. Radiat. Transf. 112 (2011) 1304.
[64] I.V. Ptashnik, T.M. Petrova, Y.N. Ponomarev, K.P. Shine, A.A. Solodov, A.M. Solodov, J. Quant. Spectrosc. Radiat. Transf. 120 (2013) 23.
[65] D. Mondelain, A. Aradj, S. Kassi, A.J. Campargue, Quant. Spectrosc. Radiat. Transf. 130 (2013) 381.
[66] I.V. Ptashnik, K.M. Smith, K.P. Shine, D.A. Newnham, Q. J. R. Meteorol. Soc. 130 (2004) 2391.
[67] S.A. Clough, M.W. Shepard, E.J. Mlawer, J.S. Delamere, M.J. Iacono, K. Cady-Pereira, S. Boukabara, P.D. Brown, J. Quant. Spectrosc. Radiat. 91 (2005) 233.
[68] I.V. Ptashnik, R.A. McPheat, K.P. Shine, K.M. Smith, R.G. Williams, J. Geophys. Res. 116 (2011) D16305.
[69] R. Fröchtenicht, M. Kaloudis, M. Koch, F. Huisken, J. Chem. Phys. 105 (1996) 6128.
[70] K. Nauta, R.E. Miller, Science 287 (2000) 293.
[71] A. Gutberlet, G. Schwaab, M.J. Havenith, Phys. Chem. A 115 (2011) 6297.
[72] L.B. Borst, A.M. Buswell, W.H. Rodebush, J. Chem. Phys. 6 (1938) 61.
[73] Y. Danten, T. Tassaing, M.J. Besnard, Phys. Chem. A 104 (2000) 9415.
[74] F.M. Nicolaisen, J. Quant. Spectrosc. Radiat. Transf. 110 (2009) 2060.
[75] K.L. Busarow, R.C. Cohen, G.A. Blake, K.B. Laughlin, Y.T. Lee, R.J. Saykally, J. Chem. Phys. 90 (1989) 3937.
[76] N. Pugliano, R.J. Saykally, J. Chem. Phys. 96 (1992) 1832.
[77] N. Pugliano, J.G. Cruzan, J.G. Loeser, R.J. Saykally, J. Chem. Phys. 98 (1993) 6600.
[78] C. Millot, A.J. Stone, Mol. Phys. Int. J. Interface Between Chem. Phys. 77 (1992) 439.
[79] C. Millot, J. Soetens, T.C.M. Costa, M.P. Hodges, A.J. Stone, J. Phys. Chem. A 102 (1998) 754.
[80] R.S. Fellers, L.B. Braly, R.J. Saykally, C.J. Leforestier, Chem. Phys. 110 (1999) 6306.
[81] R.S. Fellers, C. Leforestier, L.B. Braly, M.G. Brown, R.J. Saykally, Science 284 (1999) 945.
[82] L.B. Braly, J.D. Cruzan, K. Liu, R.S. Fellers, R.J. Saykally, J. Chem. Phys. 112 (2000) 10293.
[83] L.B. Braly, K. Liu, M.G. Brown, F.N. Keutsch, R.S. Fellers, R.J. Saykally, I.J. Introduction, Chem. Phys. 112 (2000) 10314.
[84] N. Goldman, R.S. Fellers, M.G. Brown, L.B. Braly, C.J. Keoshian, C. Leoforestier, R.J. Saykally, J. Chem. Phys. 116 (2002) 10148.
[85] C. Leforestier, F. Gatti, R.S. Fellers, R.J. Saykally, J. Chem. Phys. 117 (2002) 8710.
[86] F.N. Keutsch, L.B. Braly, M.G. Brown, H.A. Harker, P.B. Petersen, C. Leforestier, R.J. Saykally, J. Chem. Phys. 119 (2003) 8927.
[87] F.N. Keutsch, N. Goldman, H.A. Harker, C. Leforestier, R.J. Saykally, Mol. Phys. 101 (2003) 3477.
[88] H.A. Harker, F.N. Keutsch, C. Leoforestier, Y. Scribano, J.-X. Han, R.J. Saykally, Mol. Phys. 105 (2007) 497.
[89] H.A. Harker, F.N. Keutsch, C. Leforestier, Y. Scribano, J.-X. Han, R.J. Saykally, Mol. Phys. 105 (2007) 513.
[90] H. Shi, I.L. Jacobi, Surf. Sci. 317 (1994) 45.
[91] S. Andersson, C. Nyberg, C.G. Tengstal, Chem. Phys. Lett. 104 (1984) 305.
[92] H. Ogasawara, J. Yoshinobu, M. Kawai, Chem. Phys. Lett. 231 (1994) 188.
[93] M. Nakamura, Y. Shingaya, M. Ito, Chem. Phys. Lett. 309 (1999) 123.
[94] A.L. Glebov, A.P. Graham, A. Menzel, Surf. Sci. 427–428 (1999) 22.
[95] T. Mitsui, M.K. Rose, E. Fomin, D.F. Ogletree, M. Salmeron, Science 297 (2002) 1850.
[96] V. Ranea, a. Michaelides, R. Ramírez, P. de Andres, J. Vergés, D. King, Phys. Rev. Lett. 92 (2004) 136104.
[97] T. Kumagai, M. Kaizu, S. Hatta, H. Okuyama, T. Aruga, Phys. Rev. Lett. 100 (2008) 166101.
[98] W.L. Jorgensen, J. Chandrasekhar, J.D. Madura, R.W. Impey, M.L. Klein, J. Chem. Phys. 79 (1983) 926.
[99] J.R. Reimers, R.O. Watts, Chem. Phys. 85 (1984) 83.
[100] M.P. Hodges, A.J. Stone, S.S. Xantheas, J. Chem. Phys. 101 (1997) 9163.
[101] B. Jeziorski, R. Moszynski, K. Szalewicz, Chem. Rev. 94 (1994) 1887.
[102] C. Leforestier, K. Szalewicz, A.J. van der Avoird, Chem. Phys. 137 (2012) 014305.
[103] V. Babin, C. Leforestier, F.J. Paesani, Chem. Theory Comput. 9 (2013) 5395.

Anamika Mukhopadhyay graduated (B.Sc. & M.Sc. in Physics) in 2005 from Jadavpur University, Kolkata, India. She completed her PhD in 2012 from Indian Association for the Cultivation of Science (IACS), Kolkata working with Prof. Tapas Chakraborty. Her doctoral study involved investigation of excited state processes and association complex formation in select atmospherically important compounds, where she used different spectroscopic techniques (quadrupole-mass, UV photo-dissociation, FTIR and matrix-isolation spectroscopy). In 2011 she joined Prof. Richard James Saykally's group at University of California Berkeley where she pursued THz spectroscopy of water and water–hydrocarbon interaction. Presently she is working as a postdoctoral fellow at IISER Mohali with Prof. K.S. Viswanathan.

Will Cole received his B.S. in Chemistry in 2014 from the University of Toledo in Toledo, Ohio where he worked under Professor Jared Anderson. He joined Rich Saykally's group to pursue a PhD in Chemistry at the University of California, Berkeley in the summer of 2014. His doctoral research is primarily focused on applying new laser technologies to cover previously unattainable frequencies in the terahertz regime and applying them to the study of water clusters.

Rich Saykally is a co-author of over 400 publications that have been cited over 30,000 times ($H > 80$) and the recipient of over 70 honors and awards from nine different countries, recently including the J.C. Bose Lectureship from IACS-Kolkata and the Faraday Lectureship Prize from the RSC. He is a member of the National Academy of Sciences and the American Academy of Arts and Sciences, is a UC-Berkeley Distinguished Teacher, and has been active at the national level in science education. Over 150 students and postdocs have trained under his direction, many of whom hold prominent positions in academic, government, and industrial institutions. Saykally currently holds The Class of 1932 Endowed Professorship in the Department of Chemistry at University of California-Berkeley.